Restoring oscillatory behavior from amplitude death with anti-phase synchronization patterns in networks of electrochemical oscillations

Raphael Nagao, Wei Zou, Jürgen Kurths, and István Z. Kiss

Citation: Chaos **26**, 094808 (2016); doi: 10.1063/1.4954040
View online: http://dx.doi.org/10.1063/1.4954040
View Table of Contents: http://scitation.aip.org/content/aip/journal/chaos/26/9?ver=pdfcov
Published by the AIP Publishing

Restoring oscillatory behavior from amplitude death with anti-phase synchronization patterns in networks of electrochemical oscillations

Raphael Nagao,[1] Wei Zou,[2,3] Jürgen Kurths,[4,5,6,7] and István Z. Kiss[1,a)]
[1]*Department of Chemistry, Saint Louis University, 3501 Laclede Ave., St. Louis, Missouri 63103, USA*
[2]*Department of Physics, Hong Kong Baptist University, Kowloon Tong, Hong Kong, China*
[3]*School of Mathematics and Statistics, Huazhong University of Science and Technology, Wuhan 430074, China*
[4]*Potsdam Institute for Climate Impact Research, Telegraphenberg, Potsdam D-14415, Germany*
[5]*Institute of Physics, Humboldt University Berlin, Berlin D-12489, Germany*
[6]*Institute for Complex Systems and Mathematical Biology, University of Aberdeen, Aberdeen AB24 3FX, United Kingdom*
[7]*Department of Control Theory, Nizhny Novgorod State University, Gagarin Avenue 23, 606950 Nizhny Novgorod, Russia*

(Received 4 March 2016; accepted 22 April 2016; published online 30 June 2016)

The dynamical behavior of delay-coupled networks of electrochemical reactions is investigated to explore the formation of amplitude death (AD) and the synchronization states in a parameter region around the amplitude death region. It is shown that difference coupling with odd and even numbered ring and random networks can produce the AD phenomenon. Furthermore, this AD can be restored by changing the coupling type from difference to direct coupling. The restored oscillations tend to create synchronization patterns in which neighboring elements are in nearly anti-phase configuration. The ring networks produce frozen and rotating phase waves, while the random network exhibits a complex synchronization pattern with interwoven frozen and propagating phase waves. The experimental results are interpreted with a coupled Stuart-Landau oscillator model. The experimental and theoretical results reveal that AD behavior is a robust feature of delayed coupled networks of chemical units; if an oscillatory behavior is required again, even a small amount of direct coupling could be sufficient to restore the oscillations. The restored nearly anti-phase oscillatory patterns, which, to a certain extent, reflect the symmetry of the network, represent an effective means to overcome the AD phenomenon. *Published by AIP Publishing.*
[http://dx.doi.org/10.1063/1.4954040]

Oscillatory behavior underlies the functioning of many biological (e.g., sleep-wake cycle) and engineered (e.g., power grid) systems. These processes often take place in a network of units where the interaction is bidirectional (symmetrical), and because of the finite propagation rate along the coupling links there exists a delay. In such systems, when the interaction occurs through the difference between dynamical variables (diffusive coupling), the oscillatory behavior can disappear at sufficiently strong coupling at certain coupling delays. This coupling induced disappearance of oscillation, called as amplitude (AD) or oscillations (OD) death, has a detrimental effect in systems where oscillations are essential (such as in brain, climate, or power grid). In this paper, we show that the amplitude death phenomenon can be avoided, when the ideal diffusive coupling between the units is replaced or even minutely modified with a direct coupling between the units. In the given examples, when the coupling delay is large, a restoration of the oscillatory behavior occurs through complex anti-phase oscillatory synchronization patterns where the symmetry of the coupling topology plays an important role in the restored dynamics. The results are confirmed with both regular (ring) and irregular (random) networks of chemical reactions with nickel electrodissolution system and are interpreted with a prototype oscillatory model. The findings show that direct coupling among the units is favorable for generation of robust oscillatory patterns in networked units.

I. INTRODUCTION

Experiments and numerical simulations with a pair of coupled chemical oscillations showed two prominent dynamical features: synchronization, in which the phase differences of the oscillations can lock to a certain value (e.g., in-phase, out-of-phase, or anti-phase), and oscillation (OD) or amplitude (AD) death, in which the coupling results in stationary behavior.[1,2] The AD (or OD) behaviors have been reported in a variety of chemical systems (e.g., coupled Belousov-Zhabotinsky (BZ) reactors[3–5] and electrochemical reactions[6,7]) as well as in physics (e.g., thermo-optical oscillators,[8] electronic circuits[9,10]) and biology (neuroscience).[11] AD refers to the stabilization of the existing unstable (often homogeneous) steady state, where the coupling units lose oscillatory behavior and converge to the (nearly) identical steady state. Such mechanism is common in identical systems with delay,[9] or in systems with sufficiently large

a)izkiss@slu.edu

heterogeneity without delay.[12] With OD, new stable inhomogeneous steady states are generated, which are often located at the opposing positions of the original limit cycle.[4,10,11,13] In chemistry, such behavior was observed with BZ system[4] and also with electrochemical oscillators with negative coupling.[6] The bifurcation scenarios that induce AD and OD in coupled nonlinear oscillators have been well explored.[14–16]

In certain circumstances, harmful oscillations are unwanted and should be suppressed. However, in many realistic situations, oscillatory behavior plays a constructive role. Both AD and OD can be responsible for a loss of oscillatory dynamics, which may lead to some disfunctioning in the operation of the systems. In this sense, AD and OD are destructive and fatal to robustness of rhythmic behaviors, which need to be circumvented. How to revoke AD and OD to restore oscillations is of particular importance, which is also deemed as a challenging issue.[14] Recent investigations have been devoted to unveil possible methods of avoiding the onset of AD and OD,[17–19] which aim to understand the sustained oscillatory mechanisms of diverse nonlinear systems. An important conclusion is that addition of coupling, which is based on the difference between variables, often produces AD or OD behavior, while adding an even small amount of direct coupling often regains the oscillations. This technique was experimentally verified in a delayed global coupling configuration with a chemical reaction system (nickel electrodissolution)[20] and an electronic circuit.[21]

While the majority of experiments with chemical oscillators have been performed with a pair of elements, it is possible to build network of units. With the networks, further questions arise, e.g., what are the typical synchronization patterns or which types of network topologies can support AD or OD behavior. Important examples of chemical networks include BZ reactor systems,[22–24] BZ droplets,[25–28] BZ beads,[29–33] and chemomechanical[34] and electrochemical units.[35–41] Three globally coupled periodic oscillatory BZ reactors have been shown to exhibit the OD behavior.[42] AD has been reported in a population of globally coupled chaotic electrochemical oscillators with delays in between those required for desynchronization and enhanced synchrony.[43]

In this paper, we construct a network of chemical reaction units with delay in order to explore the network effects on AD and the synchronization patterns. Experiments are designed for regular networks (rings with both even and odd number of elements) and random networks. We explore the capability of these networks to produce the AD phenomenon with difference coupling, and the type of synchronization patterns that can be restored by changing the coupling types from difference (diffusive) to direct. The experimental results are motivated by theoretical studies with networks of Stuart-Landau oscillators, which predict the existence of AD behavior, and many of the symmetry features of the regained oscillations. Finally, the experimental results are compared to synchronization patterns obtained in other chemical reaction systems.

II. THEORETICAL RESULTS

We perform the stability analysis of AD in a general network of N delay-coupled Stuart-Landau oscillators

$$\dot{Z}_j(t) = \left(1 + iw - |Z_j(t)|^2\right)Z(t) + \frac{K}{d_j}\sum_{s=1}^{N} g_{js}\left(Z_s(t-\tau) - \alpha Z_j(t)\right), \quad (1)$$

where $j = 1, 2, ..., N$, $Z_j = x_j + iy_j$ and $w = 10$ are the complex amplitude and the natural frequency of the single jth oscillator, respectively, K is the coupling strength between two neighboring nodes, and τ is the propagation delay. The network topology is described by g_{js} as follows: if two nodes j and s are connected, then $g_{js} = g_{sj} = 1$, otherwise $g_{js} = g_{sj} = 0$. Self-connections are forbidden, i.e., $g_{jj} = 0$. d_j denotes the degree of node j, i.e., $d_j = \sum_{s=1}^{N} g_{js}$. It is notable that the coupling type in Eq. (1) is different from the normal form of difference coupling adopted in networks of diffusively coupled oscillators. Here, a feedback factor α $(0 \leq \alpha \leq 1)$ is introduced in the diffusive coupling. The coupling with α recovers to symmetrical diffusion for $\alpha = 1$ and direct coupling for $\alpha = 0$, thus the intermediate value of $0 < \alpha < 1$ links direct coupling and normal diffusive interaction.[20]

The condition for the onset of AD in the coupled systems, Eq. (1), can be determined from a linear stability analysis. The linearization equations of Eq. (1) around $Z_1(t) = Z_2(t) = \cdots = Z_N(t) = 0$ are

$$\dot{\xi_j}(t) = (1 + iw)\xi_j(t) + \frac{K}{d_j}\sum_{\substack{s=1 \\ s\neq j}}^{N} g_{js}\left(\xi_s(t-\tau) - \alpha\xi_j(t)\right), \quad (2)$$

where $\xi = (\xi_1, \xi_2, ..., \xi_N)^T$ and $G = \left(\frac{g_{js}}{d_j}\right)_{N\times N}$. The above linearized equations can be expressed in a compact form

$$\dot{\xi}(t) = [I_N \otimes (1 + iw - \alpha K)]\xi(t) + K(G \otimes I_n)\xi(t-\tau), \quad (3)$$

where $\otimes$ is the Kronecker product and I_m represents the $m-$dimensional unity matrix.

Note that G is a real symmetric matrix which can be diagonalized. Assume that matrix A satisfies

$$A^{-1}GA = diag(\rho_1, \rho_2, ..., \rho_N), \quad (4)$$

where ρ_i's are the eigenvalues of the matrix G, which can be ordered as

$$1.0 = \rho_1 \geq \rho_2 \geq \cdots \geq \rho_N \geq -1.0. \quad (5)$$

The smallest value of ρ_N satisfies the condition[44,45]

$$0 > -\frac{1}{N-1} \geq \rho_N \geq -1.0. \quad (6)$$

Let $\xi(t) = (A \otimes I_n)\eta(t)$, Eq. (3) can be decoupled into the following N independent equations:

$$\dot{\eta}_j(t) = (1 + iw - \alpha K)\eta_j(t) + K\rho_j\eta_j(t-\tau). \quad (7)$$

Assuming that all the perturbations obtain $\eta_j(t) \propto e^{\lambda t}$, we have the following N characteristic equations for the stability of AD:

$$\lambda = 1 + iw - \alpha K + K\rho_j e^{-\lambda\tau}, \quad j = 1, \ldots, N, \tag{8}$$

whose roots can be analytically expressed as

$$\lambda = \frac{1}{\tau} W\left(\tau\rho_j K e^{-(1+iw-\alpha K)\tau}\right) + 1 + iw - \alpha K, \tag{9}$$

where W is the Lambert function defined as the inverse of $G(\Lambda) = \Lambda e^{\Lambda}$.[46] If all the real parts of roots of Eq. (8) are negative, AD is stable. In fact, it can be shown that the AD regions are determined by only the largest and the smallest values of $\rho_0(\rho_1 = 1)$ and ρ_N.[47] Further, the boundaries of the AD regions are derived as the following four curves:

$$\tau_a = \frac{\cos^{-1}\left(\frac{\alpha K - 1}{K}\right)}{w - \sqrt{K^2 - (\alpha K - 1)^2}}, \tag{10}$$

$$\tau_b = \frac{2\pi - \cos^{-1}\left(\frac{\alpha K - 1}{K}\right)}{w + \sqrt{K^2 - (\alpha K - 1)^2}}, \tag{11}$$

$$\tau_c = \frac{2\pi - \cos^{-1}\left(\frac{\alpha K - 1}{K\rho_{N-1}}\right)}{w - \sqrt{(K\rho_{N-1})^2 - (\alpha K - 1)^2}}, \tag{12}$$

$$\tau_d = \frac{\cos^{-1}\left(\frac{\alpha K - 1}{K\rho_{N-1}}\right)}{w + \sqrt{(K\rho_{N-1})^2 - (\alpha K - 1)^2}}, \tag{13}$$

where τ_a and τ_b are from ρ_0, and τ_c and τ_d from ρ_{N-1}.

In what follows, we will validate the above analysis by considering both a ring network and an Erdos-Renyi (ER) random network.

A. *N* delay-coupled oscillators in a ring network

For ring networks with a nearest-neighbor coupling, ρ_N can be analytically obtained as

$$\rho_N = \begin{cases} -1.0, & \text{if } N \text{ is even,} \\ \cos\left(\left(1 - \frac{1}{N}\right)\pi\right), & \text{if } N \text{ is odd.} \end{cases} \tag{14}$$

As a typical example, here we only consider a ring network with $N = 11$ nodes to illustrate our study. The analytical critical curves given by Eqs. (10)–(13) are depicted in Figs. 1(a) and 1(b) for $\alpha = 1$ and $\alpha = 0.995$, respectively. The open circles denote the results obtained by numerically integrating the coupled system, Eq. (1), where the AD phenomenon is found. The figure shows that the AD regions in the (K, τ) plane are well bounded by the critical curves indicated by Eqs. (10)–(13). (At the natural frequency considered here, $w = 10$, there are no other AD regions at larger values of the delay.)

Figure 1(c) further depicts several AD islands for different values of α in the parameter space of (K, τ). We found that the AD island monotonically decreases as the value of α gradually decreases from unity. To quantify the above size variation of AD islands, we introduce a normalized size ratio $R = S_\alpha / S_{\alpha=1}$, where S_α means the area of the AD island for α and $S_{\alpha=1}$ for that of $\alpha = 1$. By definition, $R = 1$ for $\alpha = 1$. For $0 \le \alpha < 1$, R is numerically calculated and shown in Fig. 1(d). We observed that R monotonically decreases as α decreases from $\alpha = 1$, and remains at zero for all $\alpha < \alpha_{\min} = 0.75$.

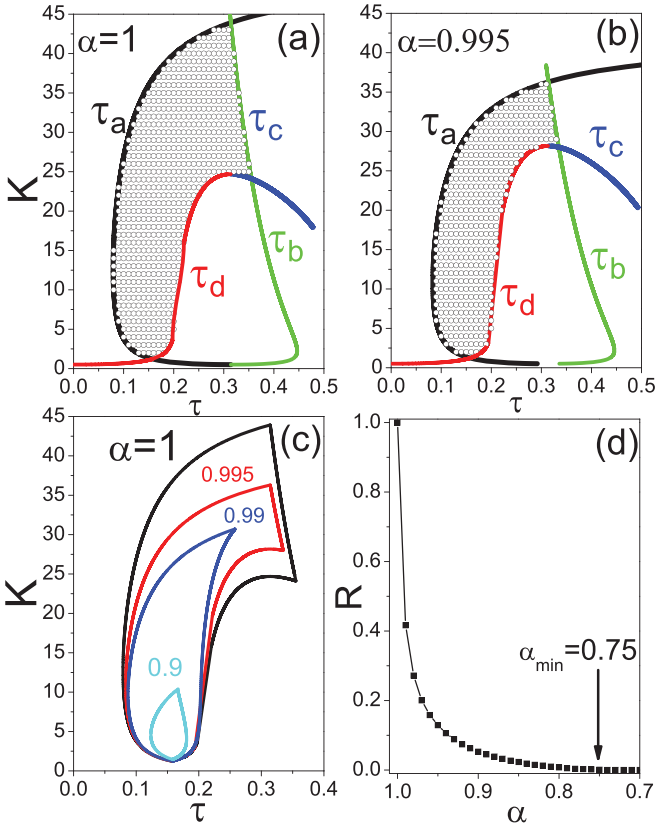

FIG. 1. AD regions with a ring of $N = 11$ nodes of Stuart-Landau oscillators. (a) and (b) AD regions in the parameter space of (τ, K) for a ring network with $N = 11$ nodes for $\alpha = 1$ and $\alpha = 0.995$, respectively. The regions of AD are enclosed by the four critical curves τ_a, τ_b, τ_c, and τ_d. The open circles represent the numerical simulations, which confirm the theoretical boundaries. (c) AD islands in the parameter space of (τ, K) for $N = 11$ Stuart-Landau oscillators on a ring network with $\alpha = 1$, 0.995, 0.99, and 0.9, respectively. (d) The normalized ratio of the area of AD island $R = S(\alpha)/S(\alpha = 1)$ versus α. R monotonically decreases with decreasing α from unity, and retains at zero for $\alpha < \alpha_{min} = 0.75$.

Figure 2(a) further illustrates the time series of the real parts of coupled Stuart-Landau oscillators with $K = 5$ and $\tau = 0.2$. The coupling was turned on at $t = 50$, after which the oscillations amplitude quickly decreased, i.e., AD occurred. After the coupling is switched from the diffusive ($\alpha = 1$) to direct ($\alpha = 0$) at $t = 250$, the established AD is indeed revoked. The enlarged view of the time-series for direct coupling $\alpha = 0$ is shown in Fig. 2(b). We find that the restored limit-cycle oscillations are nearly anti-phase type, where the phase difference between neighboring oscillators is $\frac{12\pi}{11}$.

The direct coupling with $\alpha = 0$ efficiently inhibits the occurrence of AD in the whole parameter space of time delay and coupling strength. Hence, we can conclude that the direct coupling with $\alpha = 0$ tends to favor the oscillatory

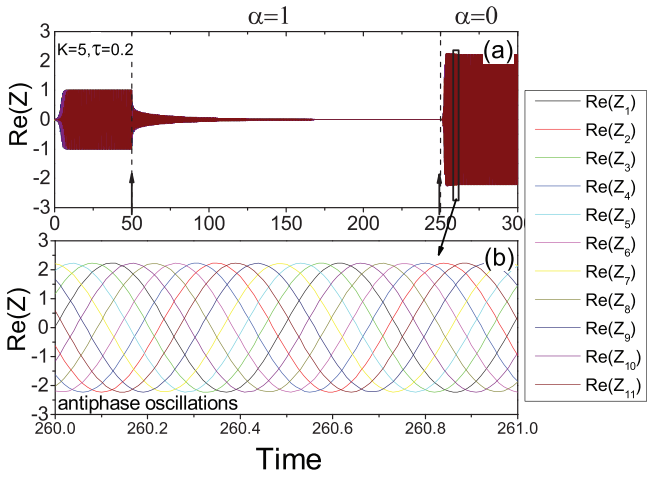

FIG. 2. AD and regained oscillations in $N=11$ delay-coupled oscillators in a ring network with $K=5$ and $\tau=0.2$. (a) The plot of time series of real parts of coupled Stuart-Landau oscillators, where the coupling strength is $K=0$ for $0<t<50$ and $K=5$ for $t\geq 50$, and the value of α is switched from $\alpha=1$ to $\alpha=0$ at $t=250$. Once the coupling is turned on for $t>50$ with $\alpha=1$, oscillation amplitudes decrease to zero, and increase again for $\alpha=0$. (b) Enlarged view of the time-series for direct coupling with $\alpha=0$ showing nearly anti-phase oscillations between two neighboring oscillators with the phase difference of $\frac{12\pi}{11}$.

activity over the difference coupling with $\alpha=1$ in ring networks.

B. *N* delay-coupled oscillators in an Erdos-Renyi network

Now we consider delay-coupled oscillators in an irregular network. Generally, for irregular networks, the smallest eigenvalue ρ_N of the corresponding matrix G cannot be analytically derived. However, ρ_N can be obtained numerically. Once ρ_N is numerically calculated, the AD regions can be plotted from Eqs. (10) to (13). As an illustrated example, here we construct a small-size ER random network with $N=11$ nodes, whose topology is schematically illustrated on the upper-right corner in Fig. 3. The ρ_N for this irregular ER network is numerically found to be -0.8677. To test the validity of the theoretical predictions, we used Eqs. (10)–(13) for the ER network to calculate the AD regions; Fig. 3 shows the results for $\alpha=0.99$. The AD regions are enclosed by the intersected area determined by the four critical curves τ_a, τ_b, τ_c, and τ_d, respectively. The theoretical AD region agrees well with numerical experiments denoted by the open circles.

Several AD islands of the irregular ER network for different values of α are further depicted in Fig. 4(a), which are obtained by directly plotting the curves given by Eqs. (10)–(13), and further confirmed by direct numerical integration. From the results shown in Fig. 4(a), again we find that by decreasing the value of α from unity, the AD island quickly shrinks in a quite similar way as previously observed in the ring network of delay-coupled oscillators in Fig. 1(c). The dependence of the normalized size ratio R of AD islands on α for the ER network is displayed in Fig. 4(b). We observe that R monotonically decreases as α decreases from unity, and acquires $R=0$ for all $\alpha<\alpha_{\min}=0.72$. This indicates that the phenomenon of AD does not occur for any values of K and τ if $\alpha<0.72$.

We further depict the time series of real parts of coupled Stuart-Landau oscillators in Fig. 5(a), where the values of $K=5$ and $\tau=0.2$ are fixed. Again, after the coupling is effective for $t>50$, oscillations amplitude quickly diminish for the ideal diffusive coupling with $\alpha=1$, where all the units are attracted to the origin in the phase space, i.e., AD occurs. However, AD is inhibited for the direct coupling with $\alpha=0$ for $t\geq 160$, and the complex patterns of regained oscillations are observed, which are shown by the enlarged view of the time-series for direct coupling $\alpha=0$ in Fig. 5(b).

Therefore, AD is impossible to be induced by the direct coupling in ER networks of delay-coupled nonlinear oscillators. From the above observations, we can lead to the following conclusion that, in the irregular ER networks of delay-coupled oscillator, the direct coupling with $\alpha=0$ is efficient to restore oscillatory behavior that are suppressed by the ideal diffusive coupling with $\alpha=1$.

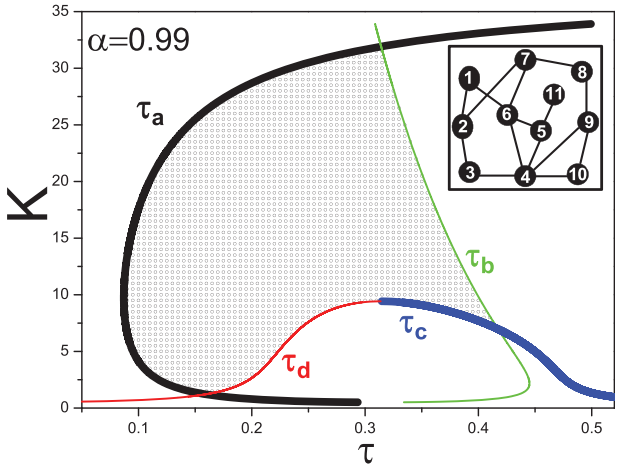

FIG. 3. AD regions in the parameter space of (τ, K) for an ER random network with $N=11$ nodes for $\alpha=0.99$. The ER random network structure is depicted in the upper-right corner. The regions of AD are bounded by the four critical curves τ_a, τ_b, τ_c, and τ_d. The open circles representing the numerical simulations confirm the theoretical boundaries.

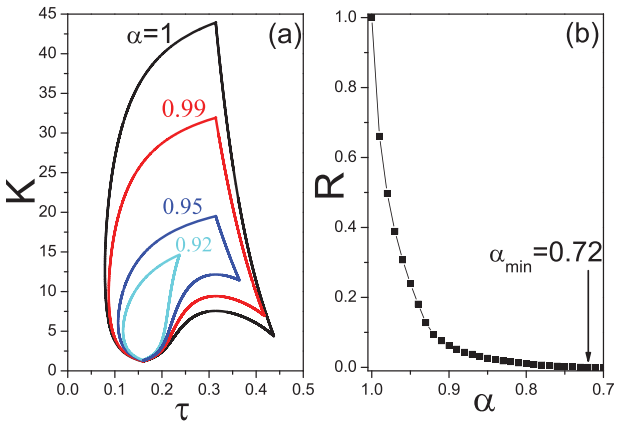

FIG. 4. AD regions for the ER random network. (a) The AD islands used in Fig. 3 for $\alpha=1, 0.99, 0.95$, and 0.92, respectively. (b) The size ratio R of AD islands as a function of α for the employed ER random network. R monotonically decreases as α decreases from unity, and becomes zero for all $\alpha<\alpha_{min}=0.72$.

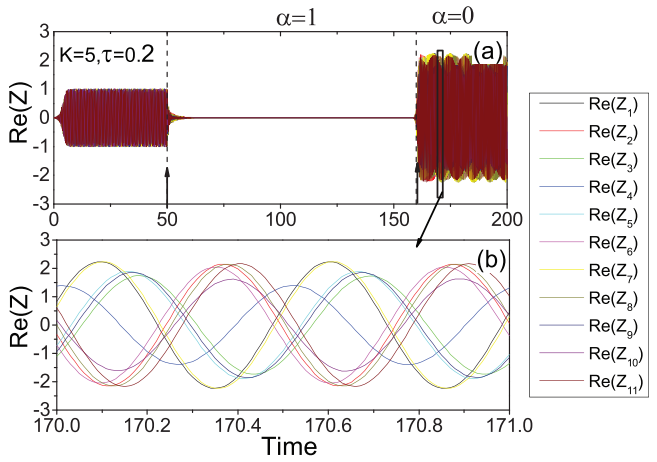

FIG. 5. AD and regained oscillations in $N = 11$ delay-coupled oscillators in the ER network with $K = 5$ and $\tau = 0.2$. (a) The plot of the time series of real parts of coupled Stuart-Landau oscillators, where the coupling strength is $K = 0$ for $0 < t < 50$ and $K = 5$ for $t \geq 50$, and the value of α is switched from $\alpha = 1$ to $\alpha = 0$ at $t = 160$. When the coupling is turned on for $t > 50$, oscillations are quenched if $\alpha = 1$, which are clearly restored for $\alpha = 0$. (b) Enlarged view of the time-series for direct coupling $\alpha = 0$ showing complex patterns of regained oscillations.

III. EXPERIMENTAL RESULTS

A. Construction of networks of delay-coupled chemical oscillatory units

The network was constructed from discrete units, each of which is a 0.69 mm diameter nickel wire, immersed in 3 mol/l sulfuric acid solution at a temperature of 10 °C (see Fig. 6). The electrode array, in which the elements are spaced in 2 mm distance within an epoxy resin, was utilized as the working electrode (WE). The circuit potential of each electrode ($V_j(t)$) can be set independently with a multichannel potentiostat (Gill-IK64, ACM Instruments) with respect to a reference electrode (RE, $Hg/Hg_2SO_4/sat.\,K_2SO_4$); the counter electrode was a 1.6 mm diameter Pt wire. (All potentials are given with respect to the RE.) The currents of the electrodes ($I_j(t)$), which are proportional to the rate of the metal dissolution process, were monitored as the observable variables with a National Instruments multifunction data acquisition card card (NI PXI-6255). A Labview based real-time data acquisition interface collected the currents and generated the circuit potentials with the chosen feedback equations that represent the interactions between the elements. The dissolution reaction exhibits oscillatory behavior due to the negative differential resistance of the process with constant circuit potential $V_0 = 1.13$ V and external resistance of 2500 Ω. The oscillations occur through a Hopf bifurcation.[48]

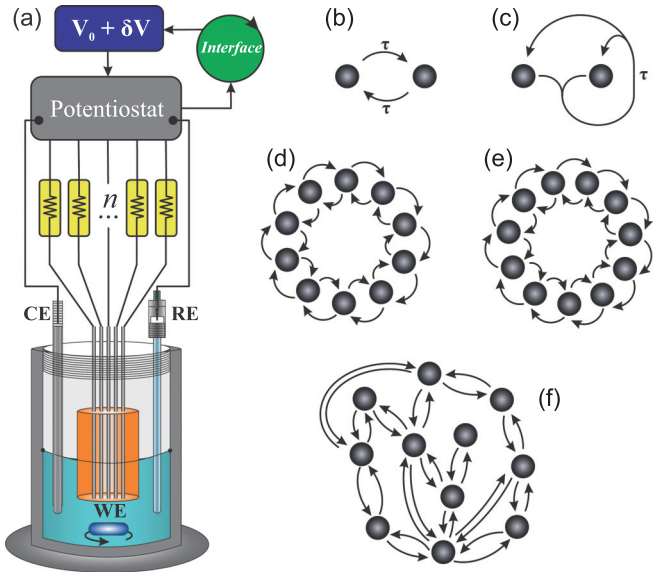

FIG. 6. Schematics for the electrochemical apparatus and network topologies. (a) WE: An array of Ni wires as the working electrode. CE: Pt counter electrode. RE: Reference electrode ($Hg/Hg_2SO_4/sat.\,K_2SO_4$). The potentiostat measures the currents and set the individual circuit potential, which is the summation of a base potential (V_0) and a feedback perturbation (δV). The feedback perturbation for each electrode depends on the currents of the electrode, which introduces the desired network interactions among the electrodes. The individual resistances attached to the wires ($R_{ind} = 2500\,\Omega$) are required to obtain the oscillations in the chemical system. Different network topologies were used: (b) two elements with local coupling, (c) two elements with global coupling, (d) ring network with even (10) nodes, (e) ring network with odd (11) nodes, and (f) random ER network with 11 nodes.

B. Comparison of global vs. local coupling with two oscillators

In a two-oscillator setting, local coupling between the elements can be implemented by setting the circuit potential ($V_j(t)$) according to Eq. (15)

$$V_j(t) = V_0 + K[\bar{I}_k(t-\tau) - \alpha \bar{I}_j(t)], \tag{15}$$

where $j, k = 1, 2 (j \neq k)$ are the oscillator indices, V_0 is the constant base potential, $\bar{I}_j(t)$ is the offset corrected current of the electrodes ($\bar{I}_j(t) = I_j(t) - o$), o is the time averaged current determined before the experiments, K is the coupling (feedback) strength, and τ is the coupling delay (see Fig. 6(b)).

Figure 7 presents an experiment, in which AD can be induced with this coupling scheme. As shown in Fig. 7(a) for $t < 100$ s, without coupling ($K = 0$) the two electrodes generate oscillatory current with slightly different frequencies ($\omega_1 = 0.343$ Hz and $\omega_2 = 0.348$ Hz). (The heterogeneity

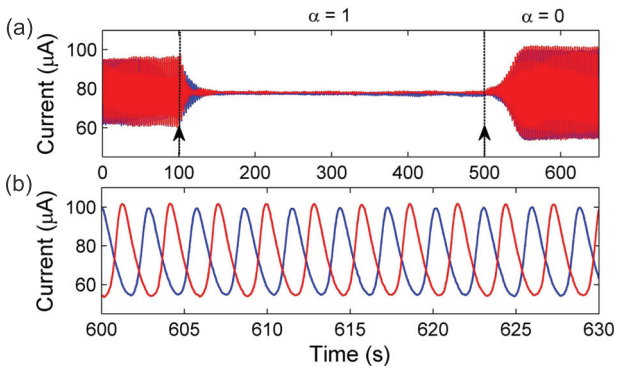

FIG. 7. Experiments: AD and regained oscillations with local coupling of two oscillators. (a) Current vs. time of the two electrodes for an experiment without coupling (phase drifting, $t < 100$ s), with difference coupling (AD behavior, $100\,\text{s} < t < 500\,\text{s}$, $K = -0.1$ V/mA, $\tau = 1.0$ s, $\alpha = 1$) and direct coupling (regained oscillations, $100\,\text{s} < t < 500\,\text{s}$, $\alpha = 0$). (b) Enlarged view of the time-series for direct coupling ($\alpha = 0$) showing anti-phase oscillations. $V_0 = 1.120$ V.

comes from slightly different surface conditions, e.g., oxide layer thickness and composition.) When the coupling was turned on ($100\text{s} < t < 500\text{s}$) with a delay of about one third of the oscillatory cycle ($\tau = 1.0\,\text{s}$, $K = -0.1\,\text{V/mA}$) AD was soon induced with difference coupling ($\alpha = 1$). As shown in Fig. 7(a), the amplitude of the oscillations was suppressed in less than 50 s. At $t = 500\,\text{s}$, the α parameter was switched to $\alpha = 0$ (direct coupling) and the oscillations were quickly restored. As a result of the direct coupling, the restored oscillations maintain a stable synchronized anti-phase state. (An enlarged view of the time-series when $\alpha = 0$ is depicted in Fig. 7(b).)

The experiments thus verify our theoretical prediction[20] that the local difference coupling between elements causes AD, and the oscillations can be regained with direct coupling in anti-phase configuration. We note that the theory predicts the existence of AD at small time delays with opposing coupling sign;[20] in that state the regaining of oscillations occurs through in-phase synchronization. We have not been able to observe this state in the experiments. It is unclear (and puzzling) why this state is unavailable experimentally. It is possible that the presence of heterogeneity and higher order nonlinearities (which are not yet considered in the theoretical treatment) could contribute the disappearance of the AD. In further experimental investigations, we consider the parameter region where AD occurs at large delay (about one third to one half of the oscillatory period).

In a previous publication,[20] a delayed global coupling scheme (see Fig. 6(c)) was proposed to investigate the effects of interactions on the oscillatory behavior. (We note that while without delay the local and global coupling schemes for two oscillators are equivalent, with delay they are different, as shown below.) The global coupling scheme can be implemented as

$$V_j(t) = V_0 + K[\langle \bar{I}(t-\tau)\rangle - \alpha \bar{I}_j(t)], \tag{16}$$

where the delayed current corresponds to a spatial mean of the individual currents: $\langle \bar{I}(t)\rangle = [\bar{I}_1(t) + \bar{I}_2(t)]/2$. This coupling configuration produces very robust AD with difference coupling ($\alpha = 1$); the results are shown in Figs. 8(a) and 8(b). In Fig. 8(a), the AD domains were experimentally monitored by changes in τ at $K = -0.5\,\text{V/mA}$. The amplitude suppression is easily obtained in the global coupling configuration. In Fig. 8(a), τ is varied by 0.1 s every 150 s. This scheme can achieve AD over a range of $\Delta\tau = 1.5\,\text{s}$. For comparison, a similar experiment was performed with the local coupling scheme (Eq. (15)) in Fig. 8(c); the AD range was diminished to $\Delta\tau = 0.5\,\text{s}$. In these experiments, we picked a feedback gain ($K = -0.5\,\text{V/mA}$), where both coupling schemes produce robust AD for a large range of K (about $K = -0.1$ to $-0.7\,\text{V/mA}$ at $\tau = 1.0\,\text{s}$ for both techniques). These results indicate that the global coupling scheme produces larger AD regions, and thus regaining oscillations in this configuration could be more crucial. This experimental result confirms the theoretical and numerical results of delayed coupled Stuart-Landau oscillators.[20]

Another important parameter in AD realization is the distance to the Hopf bifurcation that generates the oscillations. The theory and numerical simulations predicted[49] that for AD to occur, the oscillation should be sufficiently close to the Hopf bifurcation. Figs. 8(b) and 8(d) show the AD experiments for the global and local coupling schemes, respectively, for oscillation further away from the Hopf bifurcation. While the global coupling scheme produces AD, which can be restored with direct coupling, the local coupling scheme cannot produce AD. (We have performed a careful parameter search and did not find any coupling delay and coupling strength that would produce AD.) These observations further confirm the theoretical predictions[49] that for AD to occur the oscillator must be close to the Hopf bifurcation points and reinforce the idea that the global coupling scheme produces AD in larger parameter regions than the local coupling scheme.

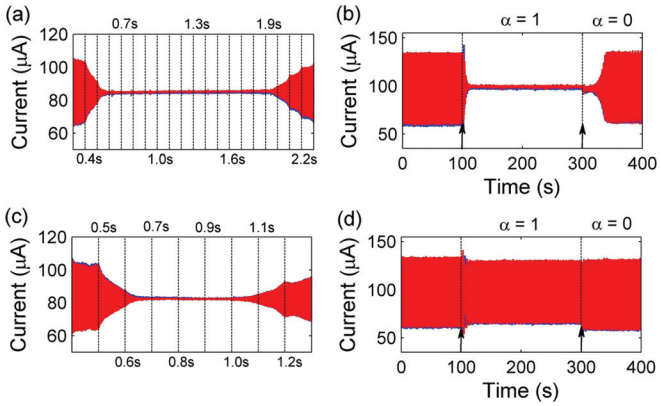

FIG. 8. Experiments: AD domains for two oscillators with global and local coupling. (a) Global coupling induced AD close to Hopf bifurcation (τ steps of 0.1 s every 150 s, $\alpha = 1$, $V_0 = 1.130\,\text{V}$). (b) Global coupling induced AD far away from Hopf bifurcation. ($100\,\text{s} < t < 300\,\text{s}$, $\tau = 1.0\,\text{s}$, $\alpha = 1$, $V_0 = 1.180\,\text{V}$). (c) Local coupling induced AD close to Hopf bifurcation (τ steps of 0.1 s every 150 s, $\alpha = 1$, $V_0 = 1.130\,\text{V}$). (d) Local coupling cannot produce AD far away from Hopf bifurcation ($100\,\text{s} < t < 300\,\text{s}$, $\tau = 1.0\,\text{s}$, $\alpha = 1$, $V_0 = 1.180\,\text{V}$). $K = -0.5\,\text{V/mA}$.

Next, we will consider the coupling schemes in between local and global coupling, i.e., network topologies; in these examples, the oscillations will occur relatively close to the Hopf bifurcation (i.e., similar to that in Fig. 8(c)) where AD occurs with difference coupling ($\alpha = 1$).

C. Amplitude death and restored oscillations with ring network topology

The local coupling topology described in Eq. (15) can be extended to multi-oscillator systems with network topologies

$$V_j(t) = V_0 + K\sum_{k=1}^{N} g_{j,k}[\bar{I}_k(t-\tau) - \alpha \bar{I}_j(t)], \tag{17}$$

where N is the number of oscillators, and the parameters $g_{j,k} = g_{k,j}$ define the network topology (as in Eq. (1)). First, we consider a ring network of $N = 10$ oscillators. Fig. 9 shows that AD is obtained with the difference coupling ($50\,\text{s} < t < 450\,\text{s}$, $\alpha = 1$) with coupling parameters similar to those used with two elements in Fig. 7. Different from two coupled oscillators, the amplitude suppression in Fig. 9(a) occurred in a slower manner, requiring around 200 s; it takes

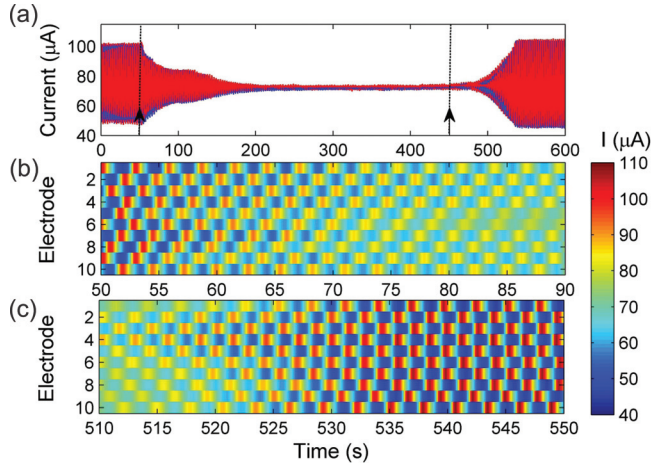

FIG. 9. Experiments: AD and regained oscillations in a ring network with 10 oscillators. (a) Current vs. time of the 10 electrodes labeled as blue (odd) and red (even) without coupling (phase drifting, $t < 50$ s), with difference coupling (AD behavior, $50\,\text{s} < t < 450\,\text{s}$, $K = -0.1\,\text{V/mA}$, $\tau = 1.0\,\text{s}$, $\alpha = 1$) and direct coupling (regained oscillations, $450\,\text{s} < t < 600\,\text{s}$, $\alpha = 0$). (b) Spatiotemporal plot for transient to AD ($K = -0.1\,\text{V/mA}$, $\tau = 1.0$ s, $\alpha = 1$). (c) Spatiotemporal plot of the restoration of oscillations ($\alpha = 0$). $V_0 = 1.123$ V.

about four times longer to reach the AD state in the ring of ten elements than for two. A spatiotemporal plot of the early stages of AD can be seen in Fig. 9(b) which shows that AD is achieved in an anti-phase pattern, where each element tends to oscillate in approximate anti-phase configuration to their neighbors. The adjustment of the phases of the oscillations is accompanied with a fast amplitude decrease as the AD state is reached. When the difference coupling is switched to direct coupling ($\alpha = 0$ at $t = 450$ s), the oscillations are regained (Fig. 9(a)) and the spatiotemporal patterns (Fig. 9(c)) exhibit an anti-phase synchronization pattern.

A detailed analysis of the restored oscillations in a ring of 10 electrochemical oscillators is shown in Fig. 10. The synchronization pattern, where each element is in nearly perfect anti-phase configuration to its neighbor, is visualized in current time-series (Fig. 10(a)), a color-coded spatio-temporal plot (Fig. 10(b)), and phase snapshots (Fig. 10(c)). This state represents an anti-phase frozen state, in which there is no rotation around the ring. Although the pattern shown in Figs. 10(a)–10(c) represents the most common form of synchronization, in some experiments we obtained another pattern shown in Figs. 10(d)–10(f). In this state, the phase difference is slightly larger than π between the neighboring elements. Because the phase difference is larger than π, every other element has a similar phase difference. As a result, we can conceive that there are two pseudo-rotational waves along the ring: one wave propagates along the odd nodes, while the other on the even nodes in a symmetrically spatial phase distribution among the oscillators. (The set of arrows inside the ring in Fig. 10(f) simplifies the dynamic visualization of the two rotational waves in this context.) Moreover, as clearly shown in Fig. 10(f), elements at the opposing position along the ring [(1, 6), (2, 7), (3, 8), (4, 9), (5, 10)] are nearly in-phase. This synchronization pattern thus represents an anti-phase rotating wave state, in which two waves are circling around the ring.

The patterns obtained with $N = 10$ oscillators can be disrupted by odd number elements; therefore, we also looked at the behavior with $N = 11$. Fig. 11 shows AD observed in

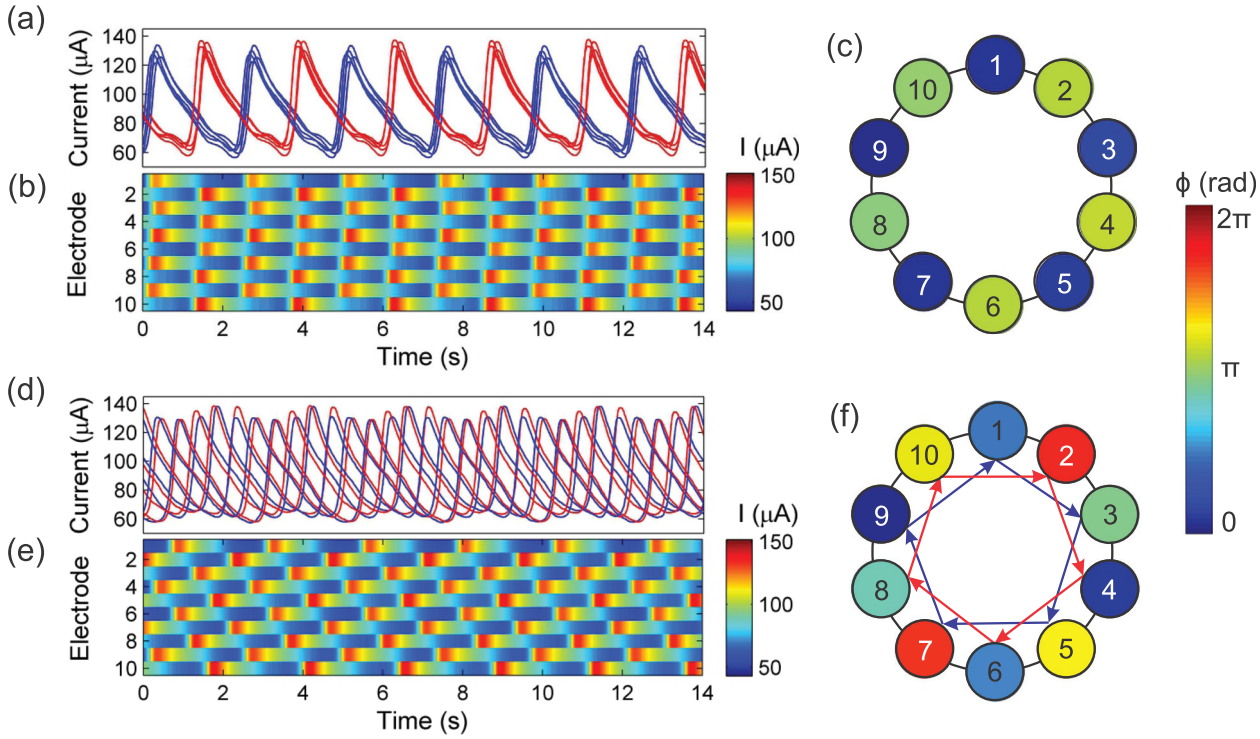

FIG. 10. Experiments: Synchrony patterns for the restored oscillations in a ring network with 10 oscillators with anti-phase frozen ((a)–(c)) and rotating ((d) and (e)) waves. ((a) and (d)) Current vs. time of the 10 electrodes labeled as blue (odd) and red (even) with direct coupling ($K = -0.1\,\text{V/mA}$, $\tau = 1.2$ s, $\alpha = 0$). ((b) and (e)) Spatiotemporal plot of the restoration of oscillations. ((c) and (f)) Snapshot of the phases of the oscillations. $V_0 = 1.180$ V.

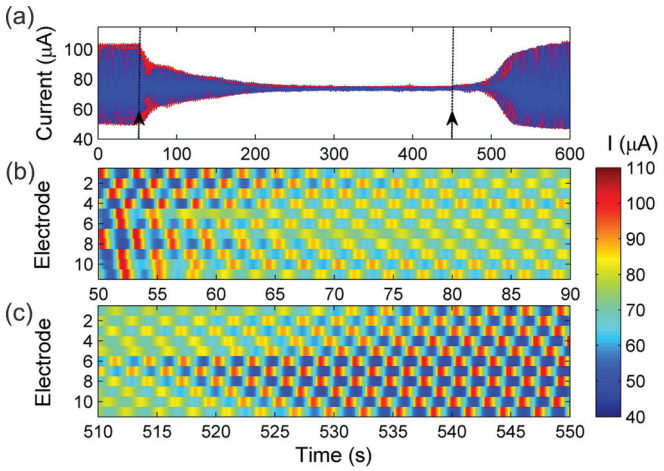

FIG. 11. Experiments: AD and regained oscillations in a ring network with 11 oscillators. (a) Current vs. time of the 11 electrodes labeled as blue (odd) and red (even) without coupling (phase drifting, $t < 50$ s), with difference coupling (AD behavior, $50\,\text{s} < t < 450\,\text{s}$, $K = -0.1$ V/mA, $\tau = 1.0$ s, $\alpha = 1$), and direct coupling (regained oscillations, $450\,\text{s} < t < 600\,\text{s}$, $\alpha = 0$). (b) Spatiotemporal plot of the AD ($K = -0.1$ V/mA, $\tau = 1.0$ s, $\alpha = 1$). (c) Spatiotemporal plot of the restoration of oscillations ($\alpha = 0$). $V_0 = 1.123$ V.

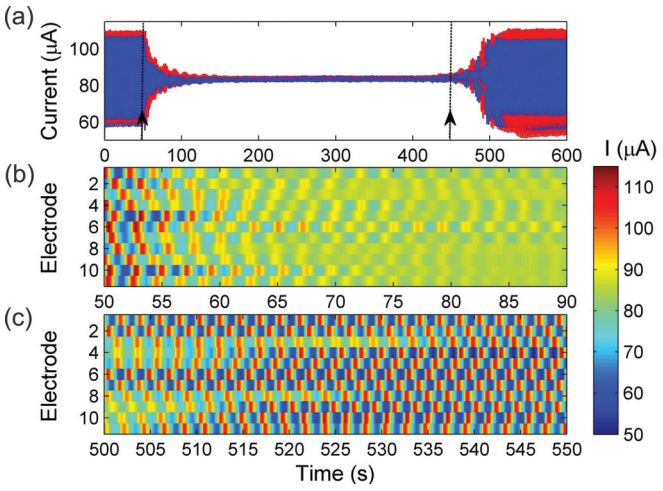

FIG. 13. Experiments: AD and regained oscillations in ER random network with 11 oscillators. (a) Current vs. time of the 11 electrodes labeled as blue (odd) and red (even) without coupling (phase drifting, $t < 50$ s), with difference coupling (AD behavior, $50\,\text{s} < t < 450\,\text{s}$, $K = -0.1$ V/mA, $\tau = 0.65$ s, $\alpha = 1$) and direct coupling (regained oscillations, $450\,\text{s} < t < 600\,\text{s}$, $\alpha = 0$). (b) Spatiotemporal plot of transient to AD ($50\,\text{s} < t < 90\,\text{s}$, $K = -0.1$ V/mA, $\tau = 1.0$ s, $\alpha = 1$). (c) Spatiotemporal plot of the restoration of oscillations ($500\,\text{s} < t < 550\,\text{s}$, $\alpha = 0$). $V_0 = 1.145$ V.

electrochemical experiments with a ring network of 11 oscillators with difference coupling ($\alpha = 1$ for $50\,\text{s} < t < 450\,\text{s}$). (The same set of parameters described with $N = 10$ in Fig. 9 was utilized in this experiment.) In Fig. 11(a), we see that, similar to the $N = 10$ case, AD is again reached in a long transient time of about 200 s. A spatiotemporal plot of the transition to the AD state in Fig. 11(b) reveals the lack of a clear anti-phase relationship between the elements; nonetheless, as time progresses an anti-phase wave starts to develop. By changing the coupling from difference ($\alpha = 1$) to direct ($\alpha = 0$, $t > 450$ s), the oscillations are quickly restored (Fig. 11(a)). While with $N = 10$ the restoration of the rhythm occurred quite uniformly (all elements started to oscillate at about the same time), with $N = 11$ the process is more heterogeneous (see Fig. 11(c)).

The synchrony pattern of the restored oscillations is shown in Fig. 12. Because of the presence of odd number of oscillators, now we can see a clear wave that rotates with a larger than π phase difference along the ring. Every other element has similar phases in such a way that the wave propagates in an alternation between odd (elements 1, 3, 5, 7, 9, 11) and even (2, 4, 6, 8, 10) nodes in each 2π-rotation. We thus see that because a non-rotational wave is not possible with $N = 11$, we typically obtain an anti-phase rotational wave with the restored oscillations.

D. Amplitude death and restored oscillations with random network topology

Finally, our experimental setup also allows the construction of random networks; we implemented the same ER network that was used in the simulations. The effectiveness to reach AD was also tested for this topology. Similar to the regular network, AD can also be achieved with the difference coupling, as shown in Fig. 13(a) ($50\,\text{s} < t < 450\,\text{s}$) with $\alpha = 1$. Compared to the behavior of the regular ring network, the AD was achieved in a relatively short time (about 100 s);

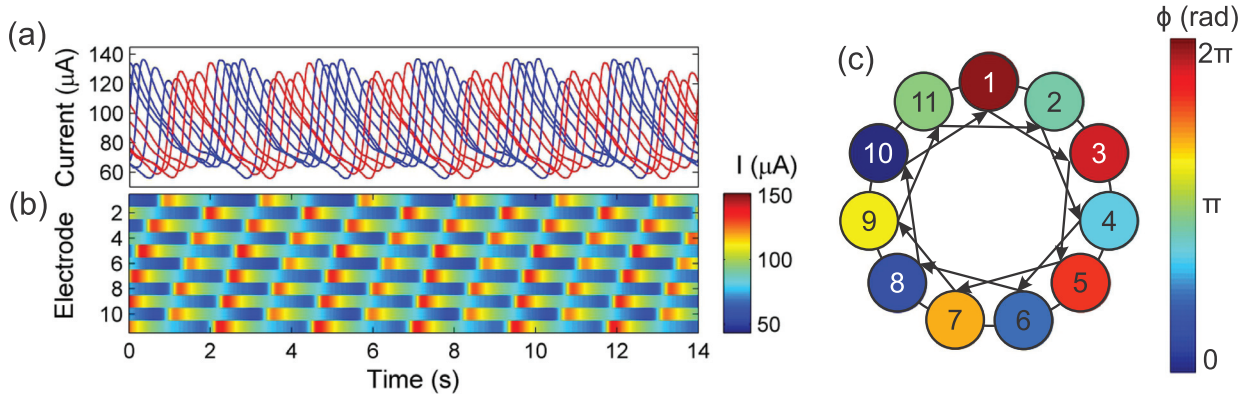

FIG. 12. Experiments: Synchronization pattern for restored oscillations in a ring network with 11 elements. (a) Current vs. time of the 11 electrodes labeled as blue (odd) and red (even) with direct coupling ($K = -0.1$ V/mA, $\tau = 1.2$ s, $\alpha = 0$). (b) Spatiotemporal plot of the restoration of oscillations. (c) Snapshot of the phases of the oscillations. $V_0 = 1.180$ V.

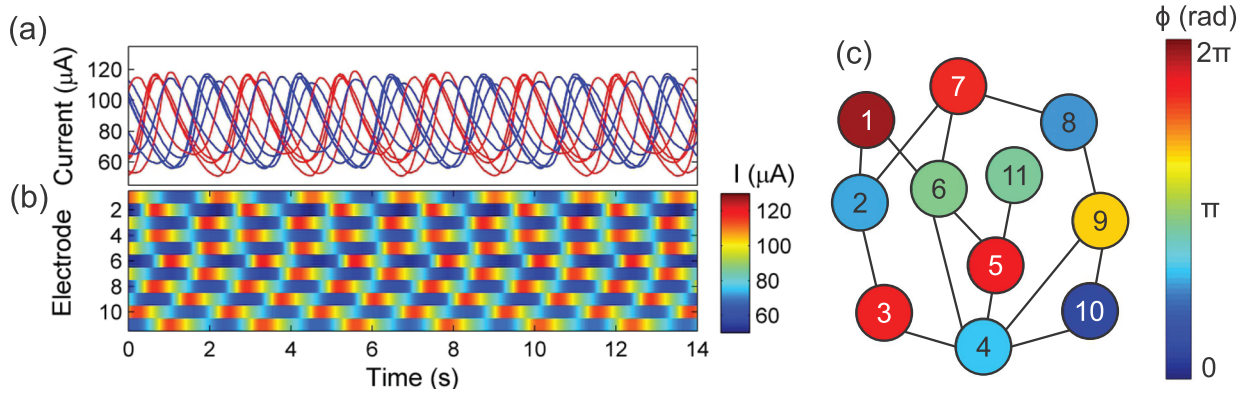

FIG. 14. Experiments: Synchrony patterns of restored oscillations in ER random network with 11 oscillators. (a) Current vs. time of the 11 electrodes labeled as blue (odd) and red (even) with direct coupling ($K = -0.1\,\mathrm{V/mA}$, $\tau = 0.5\,\mathrm{s}$, $\alpha = 0$). (b) Spatiotemporal plot of currents. (c) Snapshot of phases of the oscillations. $V_0 = 1.160\,\mathrm{V}$.

the spatiotemporal plot (Fig. 13(b)) reveals that it takes different times for the elements to reach the AD state, but it is difficult to discern a pattern in the process. The oscillations can be very quickly restored with direct coupling ($t > 450\,\mathrm{s}$ in Fig. 13(a)) and the restoration of oscillations occurred in a heterogeneous transient pattern (Fig. 13(c)). The synchrony pattern in the regained oscillations is shown in Fig. 14. Although it is difficult to find a definite structure in the pattern, we can identify some general trends. Elements that are coupled to each other tend to have different phases (e.g., close to anti-phase synchrony). Every other element along the ring segment (1, 3, 5, 7) is nearly in-phase, while every other element along the ring segment (2, 4, 8) has similar phase with a small offset, which is similar to a frozen anti-phase state. Element 11 is a "dead-end" connected to element 5, and complements the ring-segment with the frozen anti-phase synchrony. Finally, the remaining segment elements (10, 8, 6) form a rotating wave-like structure. Note that these identified pattern segments form complex loops in the network with one element in between them. We can thus conclude that the random network displays co-existence of fractured synchrony with both anti-phase frozen and rotating waves in subnetworks favorable for the development of the synchrony pattern.

IV. CONCLUSIONS

We demonstrated through theoretical analysis and chemical experiments that difference delayed coupling in a network of oscillatory elements close to a Hopf bifurcation can produce AD behavior. The investigated ring and random networks are thus capable of facilitating the coupling signal propagation for the amplitude dampening. When the coupling was changed from diffusive to direct, the AD state loses stability and oscillatory patterns are obtained. The experiments show that destruction of the AD state occurs through nearly anti-phase synchrony patterns, where the neighboring oscillators typically have large phase difference ($\geq \pi$). The patterns can be either frozen (e.g., anti-phase relationship) or propagating (larger than anti-phase relationship).

The observed rotating waves show similarities to those observed with BZ microdroplet system.[28] We note that in that example the patterns are obtained with nearly zero delay coupling through the inhibitor variable. The rotating waves presented here were obtained with delayed coupling of the currents of the electrodes, which relate the activator variables of the electrochemical system (the electrode potentials). With non-delayed coupling in the electrochemical system (with the use of a resistance network interface), in-phase frozen or rotating waves have been observed.[40] In a distributed electrochemical system with a ring electrode, a rotating multi-cluster state was observed with strong local positive, and weak negative local coupling.[50] The experimental results presented here thus contribute to the large variety of fundamentally different rotating waves that can be observed in chemical reaction systems.

ACKNOWLEDGMENTS

We acknowledge the financial support from the National Natural Science Foundation CHE-1465013 and Grant No. 229171/2013-3 (CNPq). W.Z. was supported by Hong Kong Scholars Program.

[1]A. Pikovsky, M. Rosenblum, and J. Kurths, *Synchronization: A Universal Concept in Nonlinear Sciences* (Cambridge University Press, Cambridge, 2001).
[2]M. Wickramasinghe and I. Z. Kiss, "Synchronization of electrochemical oscillators," in *Engineering of Chemical Complexity*, edited by A. S. Mikhailov and G. Ertl (Wolrd Scientific, 2013), pp. 215–236.
[3]K. Bar-Eli and S. Reuveni, "Stable stationary states of coupled chemical oscillators. Experimental evidence," J. Phys. Chem. **89**, 1329–1330 (1985).
[4]M. F. Crowley and I. R. Epstein, "Experimental and theoretical studies of a coupled chemical oscillator: Phase death, multistability, and in-phase and out-of-phase entrainment," J. Phys. Chem. **93**, 2496–2502 (1989).
[5]M. Yoshimoto, "Phase-death mode in two-coupled chemical oscillators studied with reactors of different volume and by simulation," Chem. Phys. Lett. **280**, 539–543 (1997).
[6]S. Jain, I. Z. Kiss, J. Breidenich, and J. L. Hudson, "The effect of IR compensation on stationary and oscillatory patterns in dual-electrode metal dissolution systems," Electrochim. Acta **55**, 363–373 (2009).
[7]Y. Zhai, I. Z. Kiss, and J. L. Hudson, "Amplitude death through a Hopf bifurcation in coupled electrochemical oscillators: Experiments and simulations," Phys. Rev. E **69**, 026208 (2004).
[8]R. Herrero, M. Figueras, J. Rius, F. Pi, and G. Orriols, "Experimental observation of the amplitude death effect in two coupled nonlinear oscillators," Phys. Rev. Lett. **84**, 5312–5315 (2000).

[9]D. V. Ramana Reddy, A. Sen, and G. L. Johnston, "Experimental evidence of time-delay-induced death in coupled limit-cycle oscillators," Phys. Rev. Lett. **85**, 3381–3384 (2000).
[10]T. Banerjee and D. Ghosh, "Experimental observation of a transition from amplitude to oscillation death in coupled oscillators," Phys. Rev. E **89**, 062902 (2014).
[11]G. B. Ermentrout and N. Kopell, "Oscillator death in systems of coupled neural oscillators," SIAM J. Math. Anal. **50**, 125 (1990).
[12]D. G. Aronson, G. B. Ermentrout, and N. Kopell, "Amplitude response of coupled oscillators," Physica D **41**, 403–449 (1990).
[13]A. Koseska, E. Volkov, and J. Kurths, "Transition from amplitude to oscillation death via Turing bifurcation," Phys. Rev. Lett. **111**, 024103 (2013).
[14]G. Saxena, A. Prasad, and R. Ramaswamy, "Amplitude death: The emergence of stationarity in coupled nonlinear systems," Phys. Rep. **521**, 205 (2012).
[15]A. Koseska, E. Volkov, and J. Kurths, "Oscillation quenching mechanisms: Amplitude vs. oscillation death," Phys. Rep. **531**, 173 (2013).
[16]K. Bar-Eli, "Oscillations death revisited; coupling of identical chemical oscillators," Phys. Chem. Chem. Phys. **13**, 11606–11614 (2011).
[17]K. Konishi, "Limitation of time-delay induced amplitude death," Phys. Lett. A **341**, 401–409 (2005).
[18]W. Zou, C. Yao, and M. Zhan, "Eliminating delay-induced oscillation death by gradient coupling," Phys. Rev. E **82**, 056203 (2010).
[19]W. Zou, D. V. Senthilkumar, M. Zhan, and J. Kurths, "Reviving oscillations in coupled nonlinear oscillators," Phys. Rev. Lett. **111**, 014101 (2013).
[20]W. Zou, D. V. Senthilkumar, R. Nagao, I. Z. Kiss, Y. Tang, A. Koseska, J. Duan, and J. Kurths, "Restoration of rhythmicity in diffusively coupled dynamical networks," Nat. Commun. **6**, 7709 (2015).
[21]D. Ghosh, T. Banerjee, and J. Kurths, "Revival of oscillation from mean-field-induced death: Theory and experiment," Phys. Rev. E **92**, 052908 (2015).
[22]W. Hohmann, N. Schinor, M. Kraus, and F. W. Schneider, "Electrically coupled chemical oscillators and their action potentials," J. Phys. Chem. A **103**, 5742–5748 (1999).
[23]V. Horvath, P. L. Gentili, V. K. Vanag, and I. R. Epstein, "Pulse-coupled chemical oscillators with time delay," Angew. Chem. Int. Ed. **51**, 6878–6881 (2012).
[24]V. Votrubova, P. Hasal, L. Schreiberova, and M. Marek, "Dynamical patterns in arrays of coupled chemical oscillators and excitators," J. Phys. Chem. A **102**, 1318–1328 (1998).
[25]J. Delgado, N. Li, M. Leda, H. O. Gonzalez-Ochoa, S. Fraden, and I. R. Epstein, "Coupled oscillations in a 1D emulsion of Belousov-Zhabotinsky droplets," Soft Matter **7**, 3155–3167 (2011).
[26]M. Toiya, H. O. Gonzalez-Ochoa, V. K. Vanag, S. Fraden, and I. R. Epstein, "Synchronization of chemical micro-oscillators," J. Phys. Chem. Lett. **1**, 1241–1246 (2010).
[27]M. Toiya, V. K. Vladimir, and I. R. Epstein, "Diffusively coupled chemical oscillators in a microfluidic assembly," Angew. Chem. Int. Ed. **47**, 7753–7755 (2008).
[28]N. Tompkins, N. Li, C. Girabawe, M. Heymann, G. B. Ermentrout, I. R. Epstein, and S. Fraden, "Testing Turing's theory of morphogenesis in chemical cells," Proc. Natl. Acad. Sci. U.S.A. **111**, 4397–4402 (2014).
[29]S. Nkomo, M. R. Tinsley, and K. Showalter, "Chimera states in populations of nonlocally coupled chemical oscillators," Phys. Rev. Lett. **110**, 244102 (2013).
[30]M. R. Tinsley, S. Nkomo, and K. Showalter, "Chimera and phase-cluster states in populations of coupled chemical oscillators," Nat. Phys. **8**, 662–665 (2012).
[31]A. F. Taylor, M. R. Tinsley, F. Wang, and K. Showalter, "Phase clusters in large populations of chemical oscillators," Angew. Chem. Int. Ed. **50**, 10161–10164 (2011).
[32]A. F. Taylor, M. R. Tinsley, F. Wang, Z. Y. Huang, and K. Showalter, "Dynamical quorum sensing and synchronization in large populations of chemical oscillators," Science **323**, 614–617 (2009).
[33]R. Makki, A. P. Munuzuri, and J. Perez-Mercader, "Periodic perturbation of chemical oscillators: Entrainment and induced synchronization," Chem. Eur. J. **20**, 14213–14217 (2014).
[34]P. Kumar, D. K. Verma, P. Parmananda, and S. Boccaletti, "Experimental evidence of explosive synchronization in mercury beating-heart oscillators," Phys. Rev. E **91**, 062909 (2015).
[35]M. Wickramasinghe and I. Z. Kiss, "Spatially organized dynamical states in chemical oscillator networks: Synchronization, dynamical differentiation, and chimera patterns," PLoS One **8**, e80586 (2013).
[36]J. Nawrath, M. C. Romano, M. Thiel, I. Z. Kiss, M. Wickramasinghe, J. Timmer, J. Kurths, and B. Schelter, "Distinguishing direct from indirect interactions in oscillatory networks with multiple time scales," Phys. Rev. Lett. **104**, 038701 (2010).
[37]I. Z. Kiss, Y. M. Zhai, and J. L. Hudson, "Emerging coherence in a population of chemical oscillators," Science **296**, 1676–1678 (2002).
[38]K. Blaha, J. Lehnert, A. Keane, T. Dahms, P. Hövel, E. Schöll, and J. L. Hudson, "Clustering in delay-coupled smooth and relaxational chemical oscillators," Phys. Rev. E **88**, 062915 (2013).
[39]A. Karantonis, Y. Miyakita, and S. Nakabayashi, "Synchronization of coupled assemblies of relaxation oscillatory electrode pairs," Phys. Rev. E **65**, 046213 (2002).
[40]M. Sebek, R. Toenjes, and I. Z. Kiss, "Complex rotating waves and long transients in a ring network of electrochemical oscillators with sparse random cross-connections," Phys. Rev. Lett. **116**, 068701 (2016).
[41]M. Wickramasinghe and I. Z. Kiss, "Spatially organized partial synchronization through the chimera mechanism in a network of electrochemical reactions," Phys. Chem. Chem. Phys. **16**, 18360–18369 (2014).
[42]M. Yoshimoto, K. Yoshikawa, and Y. Mori, "Coupling among three chemical oscillators: Synchronization, phase death, and frustration," Phys. Rev. E **47**, 864–874 (1993).
[43]Y. Zhai, I. Z. Kiss, and J. L. Hudson, "Control of complex dynamics with time-delayed feedback in populations of chemical oscillators: Desynchronization and clustering," Ind. Eng. Chem. Res. **47**, 3502–3514 (2008).
[44]F. M. Atay, "Oscillator death in coupled functional differential equations near Hopf bifurcation," J. Differ. Equations **221**, 190 (2006).
[45]W. Michiels and H. Nijmeier, "Synchronization of delay-coupled nonlinear oscillators: An approach based on the stability analysis of synchronized equilibria," Chaos **19**, 033110 (2009).
[46]J. K. Hale, *Functional Differential Equations* (Springer, New York, 1971).
[47]M. P. Mehta and A. Sen, "Death island boundaries for delay-coupled oscillator chains," Phys. Lett. A **355**, 202–206 (2006).
[48]I. Z. Kiss, Z. Kazsu, and V. Gáspár, "Tracking unstable steady states and periodic orbits of oscillatory and chaotic electrochemical systems using delayed feedback control," Chaos **16**, 033109 (2006).
[49]W. Zou, X. Zheng, and M. Zhan, "Insensitive dependence of delay-induced oscillation death on complex networks," Chaos **21**, 023130 (2011).
[50]H. Varela, C. Beta, A. Bonnefont, and K. Krischer, "A hierarchy of global coupling induced cluster patterns during the oscillatory H_2-electrooxidation reaction on a Pt ring-electrode," Phys. Chem. Chem. Phys. **7**, 2429–2439 (2005).